Available online at www.sciencedirect.com
ScienceDirect
Journal of Power Sources 161 (2006) 723–729
JOURNAL OF POWER SOURCES
www.elsevier.com/locate/jpowsour

Electrochemical characteristics and impedance spectroscopy studies of nano-cobalt silicate hydroxide for supercapacitor

Guo-Qing Zhang [b], Yong-Qing Zhao [b], Feng Tao [b], Hu-Lin Li [a,b,*]

[a] College of Material Science and Engineering, Nanjing University of Aeronautics and Astronautics, Nanjing 210016, PR China
[b] College of Chemistry and Chemical Engineering, Lanzhou University, Lanzhou 730000, PR China

Received 17 January 2006; received in revised form 20 March 2006; accepted 22 March 2006
Available online 2 May 2006

Abstract

Cobalt silicate hydroxide ($Co_3[Si_2O_5]_2[OH]_2$) was prepared by chemical method for use in electrochemical capacitors. X-ray diffraction (XRD) and transmission electron microscopy (TEM) tests indicate that the material was pure hexagonal phase with uniform nanometer size distribution. Cyclic voltammeter (CV) and galvanostatic charge/discharge measurements show that the cobalt silicate hydroxide-based electrode has stable electrochemical capacitor properties between potential range of 0.1–0.55 V with a maximum specific capacitance of 237 F g^{-1} in alkaline solution and 95% of capacity efficiency was reached after 150 cycles. Electrochemical impedance spectra (EIS) investigation illustrates that the capacitance of the test electrode was mainly consisted of pseudo-capacitance, which was caused by underpotential deposition of H_3O^+ at the electrode surface.

Keywords: Cobalt silicate hydroxide; Supercapacitor; Electrochemical impedance spectroscopy

1. Introduction

Much work has been done for the last 10 years on supercapacitors, as their electrochemical properties make these systems act as intermediate power and energy sources between electrochemical batteries and dielectric capacitors [1–3]. Moreover, as a new kind of energy storage device, the supercapacitor has long cycle life, high efficiency, and is environmentally friendly. Electrochemical capacitor combining the advantages of dielectric capacitors, which can deliver high power within a very short time, and rechargeable batteries, which can store high amounts of energy, have found increasingly important role in power source applications such as hybrid electric vehicles short-term power sources for mobile electric devices, etc. [4].

The electrochemical capacitors are generally classified into two types: (i) pseudo-capacitance and (ii) double-layer. There are many materials that are under close scrutiny for use as electrode materials for supercapacitor applications such as high-surface-area carbon materials [5–7], transition metal oxides [8–10], and electronically conducting polymers [11]. At the carbon surface, the capacitance is mainly from electrostatic double-layer charging. Carbon–carbon systems function on the basis of the Gouy–Chapmann and Stern–Geary electrochemical double-layer theory [12]. The charge is stored through the adsorption of the electrolyte ions on large-surface-area activated carbon (2300 m^2 g^{-1}). There is no charge-transfer reaction occurring during the charge–discharge process. The specific capacitance SC value of the activated carbon was about 125 F g^{-1} [13]. At metal oxides, it arose from redox pseudo-capacitance couple with double-layer capacitance. The hydrous ruthenium oxide was reported as the most promising materials with SC value of 863 F g^{-1} [14]. Even though noble-metal oxides or hydrous oxide (i.e. ruthenium oxides) and carbon nanotubes yield remarkably high specific capacitance and/or power densities, capacitors based on these materials are much more costly than other technologies [15–18]. Conducting polymer capacitors have been reported to display high power densities, but their specific capacitance is much lower than that of carbon/carbon and metal oxide capacitors. Thus, it is extreme important to develop alternative electrode material with a combination of cost and improved performances, which still remains a challenge to electrochemical researchers for supercapacitor practical applications.

* Corresponding author. Tel.: +86 931 891 2517; fax: +86 931 891 2582.
E-mail address: lihl@lzu.edu.cn (H.-L. Li).

0378-7753/$ – see front matter © 2006 Published by Elsevier B.V.
doi:10.1016/j.jpowsour.2006.03.041

For many years, intense research has focused on new types of silicates because of their great potentials in many areas, such as selective catalysis, molecular sieves, and gas adsorption and separation [19–27]. However, there are not reports about the electrochemical properties of this material. Herein we demonstrate cobalt silicate hydroxide nanomaterial with obvious electrochemical capacitor characteristics and high specific capacitance, which was confirmed by a series of electrochemical experiments. Electrochemical impedance spectroscopy is a useful method to obtain information about the electrode process. Impedance analysis has been utilized to understand the resistance and specific capacitance of single-cell [28] and half-cell electrodes [29] for electrochemical capacitor application. However, discussion so far has been confined to the assessment of the specific capacitance or change in the electrolyte resistance. In this study, the capacitor frequency response of cobalt silicate hydroxide as a function of the applied potential have been evaluated and the origin of capacitance of this material was also discussed in detail by means of analyzing electrochemical impedance spectroscopy.

2. Experimental

2.1. Preparation of nano-cobalt silicate hydroxide $Co_3[Si_2O_5]_2[OH]_2$

Nano-cobalt silicate hydroxide ($Co_3[Si_2O_5]_2[OH]_2$) was prepared by a hydrothermal process in a mixed water/ethanol solvent system. $Co(NO_3)$ (0.5 g) was dissolved in a mixture of distilled water (5 mL) and ethanol (20 mL), then Na_2SiO_3 (5 mL, 0.5 M) was added to form a precipitate, which was transferred into a Teflon-lined autoclave and hydrothermal treated at 180–200 °C for 2 days. The as-obtained precipitates were filtered and washed with distilled water to remove ions possibly remaining in the final products, dried at 70 °C in air and then got black powder. The products' crystal structure was characterized by X-ray diffraction (XRD, Max, M18Xce, Japan) with Cu Kα radiation (λ = 1.54178 Å) operating at 50.0 kV and 200.0 mA,employing well-ground samples at a scan rate of 0.02 ° S^{-1} in the 2θ range of 10–90°. Morphology of the as-synthesized material was investigated by transmission electron microscopy (TEM) (Hitachi-600, Japan) investigations.

Electrodes for electrochemical capacitors were prepared by mixed the active materials with 25 wt.% acetylene black and 5 wt.% PTFE (polytetrafluoroethylene) of the total electrode mass. A small amount of water was then added to this composite to make a more homogeneous mixture, which was pressed on nickel grid (1.2×10^7 MPa). The loading of the electrode was typically in the range of 24 mg cm^{-2}. All electrochemical measurements were carried out in a three electrode arrangement in 6 M KOH electrolyte. The prepared electrode was used as working electrode, a platinum foil of the same area as counter electrode. All potential were referred to Hg/HgO reference electrode coupled with a luggin capillary in the same electrolyte. Electrochemical performance was evaluated by cyclic voltammetry (CV) using CHI660 electrochemical workstation with a voltage scan rate ranging from 2 to 20 mV s^{-1}. The charge/discharge cycling properties of the electrode at constant current were evaluated with an Arbin battery tester BT2000 in the certain range of potential. Electrochemical impedance spectroscopy measurements of the prepared electrode were carried out with CHI660 electrochemical workstation in different applied potential conditions with the frequency range of 10^5 to 10^{-2} Hz taking 10 points per decade.

3. Results and discussion

3.1. Physical characteristics

The XRD pattern of cobalt silicate hydroxide ($Co_3[Si_2O_5]_2[OH]_2$) was shown in Fig. 1. The XRD patterns were successfully indexed based on the materials' structure, which exhibited the characteristic peaks of cobalt silicate hydroxide ($Co_3[Si_2O_5]_2[OH]_2$). All of the reflection patterns in Fig. 1 can been readily indexed to that of a pure hexagonal phase of $Co_3[Si_2O_5]_2[OH]_2$ with lattice constants $a = 5.33$ Å, $b = 9.19$ Å and $c = 9.25$ Å. The apparent broadening of peaks indicates the small crystal sizes of the obtained particles.

It would be interesting to examine the morphology of the material, which has been in the form of powders. From TEM images in Fig. 2, it can be seen that the material tends to form particle morphology. As estimated from TEM images, the particle size of the cobalt silicate hydroxide is among several nanometers range. Especially, the size distribution is substantial uniform. Small and uniform particle size might exhibit high surface area, which may be favorable for the supercapacitor application.

3.2. Cycle voltammetry measurements

Fig. 3 shows CV curves from nano-cobalt silicate hydroxide ($Co_3[Si_2O_5]_2[OH]_2$))-based electrode in 6 M KOH solution at low and high voltage scan rates in the range of 0.1–0.65 V. The shape of the CV curves reveal that the capacitive characteristic is very distinguished from that of electric double-layer capacitance

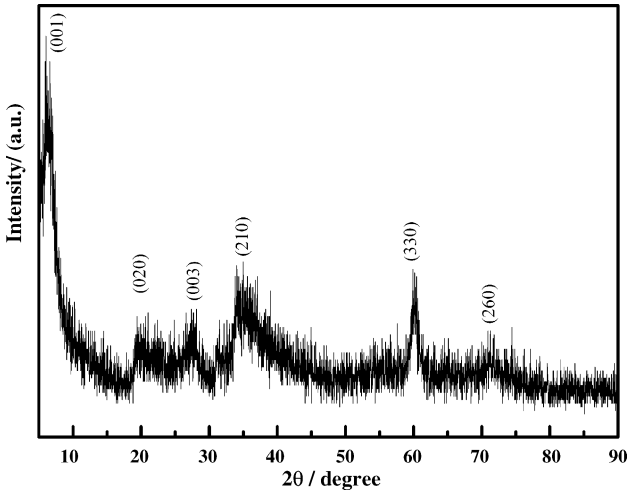

Fig. 1. XRD of nano-cobalt silicate hydroxide ($Co_3[Si_2O_5]_2[OH]_2$).

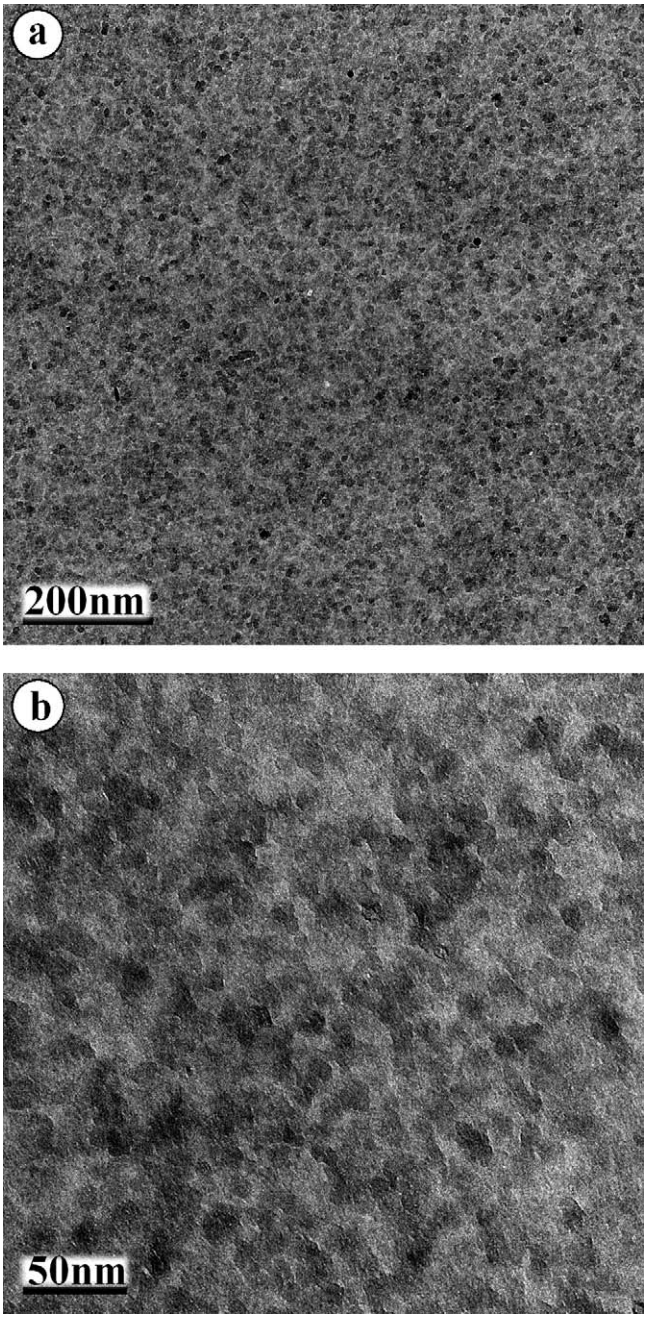

Fig. 2. TEM morphologies of nano-cobalt silicate hydroxide: (a) 25 × 1000; (b) 80 × 1000.

in which case it is normally close to an ideal rectangular shape, indicating that the capacity mainly results from the pseudo capacitive capacitance. After careful examining individual electric couples involved in the test system, we found that the potentials of Co^{2+}/Co (−0.277 V versus NHE) and K^+/K (−2.925 V versus NHE) are far from the tested voltage range. And the potential of redox reaction of $H_3O^+ + M + e \leftrightarrow M/H_{ads} + H_2O$ (0 V versus NHE) is the nearest value to the examined peak potential (0.4 V). Thus, we speculate that the redox peaks shown in CV experiments can be explained using the point of H_3O^+ underpotential deposition. Further evidence confirming this speculation can be seen in the discussion of electrochemical impedance spectra.

3.3. Charge–discharge cycling performance measurements

In order to get information about the ability of the nano-cobalt silicate hydroxide as an electrode material in supercapacitor, constant current charge/discharge measurement was carried out in aqueous media with 6 M KOH as a supporting electrolyte. Fig. 4 shows the constant current charge/discharge curve of the nano-cobalt silicate hydroxide electrode in a three-electrode system. The cut-off voltage of charging/discharging was 0.1–0.55 V with 5.7 mA cm^2 constant current density at room temperature. During the charging and discharging steps, the curve obviously display two variation range, a perfect linear variation of the time dependence of the potential (below about 0.4 V) indicate pure double-layer capacitance behavior, which was caused by the charge separation taking place between the electrode and electrolyte interface [30], and a slop variation of the time dependence of the potential (0.4–0.55 V) indicate a typical pseudo-capacitance behavior, which resulted from the electrochemical adsorption/adsorption or redox reaction at an interface between electrode and electrolyte. So, the special capacitance of the electrode is the summation of electric double-layer and pseudo-capacitance, and reached 237 F g^{-1}. The specific capacitance was obtained from $C = It/\Delta Vw$, where I and t, respectively, indicate the constant current that is applied and the time of charge/discharge, w represents the mass of electro active material.

The coulomb efficiency (η) of the electrode during charge/discharge is also shown in Fig. 5, which is calculated according to $\eta = (t_D/t_C) \times 100$, t_D and t_C are the expressions of discharge and charge times. The result reveals that the nano-cobalt silicate hydroxide electrode has a very stable coulomb efficiency about 95% over 150 cycles, which means good cycle properties for nano-cobalt silicate hydroxide as a type of supercapacitor material.

3.4. Electrochemical impedance spectroscopy analysis

The impedance of an electrochemical system is measured by applying a low-amplitude alternative voltage ΔV to a steady-state potential V_s, with $\Delta E(\omega) = \Delta E_{max}\, e^{i\omega t}$, where ω is the pulsation and ΔV_{max} is the signal amplitude. The resulted output current ΔI is a sinusoidal signal, with $\Delta I(\omega) = \Delta I_{max}\, e^{i(\omega t+\varphi)}$, where φ is the phase angle of the current versus the voltage and ΔI_{max} the signal amplitude. The electrochemical impedance $Z(\omega)$ is defined as $Z(\omega) = \Delta E/\Delta I = |Z(\omega)|\, e^{-i\varphi} = Z' + iZ''$, where Z' and Z'' are the real part and the imaginary part of the impedance, respectively, $|Z(\omega)|$ is module defined as $Z'^2 + Z''^2 = |Z(\omega)|^2$ [31].

Electrochemical impedance spectra (EIS) for nano-cobalt silicate hydroxide electrode were carried out at various potentials of interest over the capacitor operating potential range. As can be seen in Fig. 6, the Nyquist plots at 0.13, 0.24, 0.26, 0.4, 0.6 V display obviously different electrochemical characteristics, suggesting different processes occurring on the electrode. With the

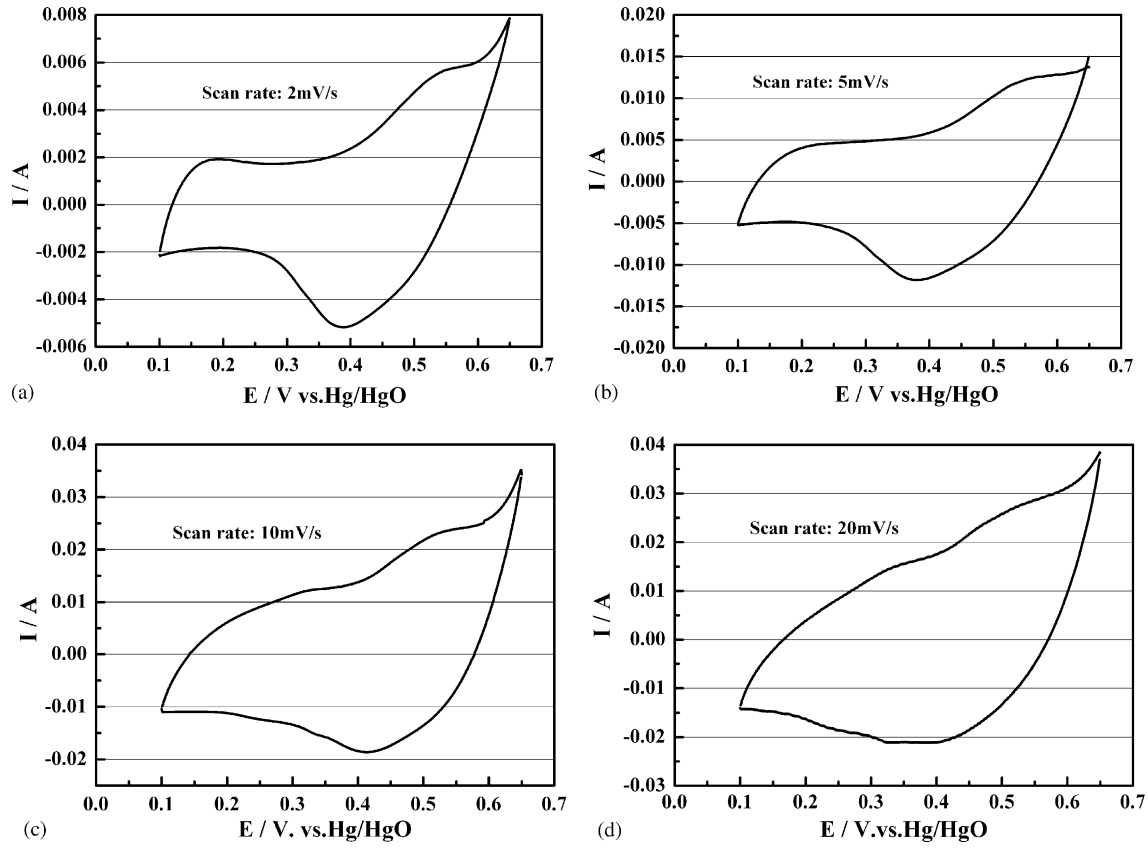

Fig. 3. Cyclic voltammograms of nano-cobalt silicate hydroxide in 6 M KOH solution at scan rate: (a) 2 mV s^{-1}; (b) 5 mV s^{-1}; (c) 10 mV s^{-1}; (d) 20 mV s^{-1}.

potential tested increasing, not only the imaginary part of the impedance sharply decreases except that of at 0.6 V and the plot tends to a vertical line, but also two obvious half circles are gradually appeared. The first circle is related to the capacitance of electric double-layer between electrode and electrolyte, which can be analogous to carbon-based electrode systems [32,33]. The second circle is the capacitance relative to faradic reaction. The complex-plane impedance plots (Fig. 6(b)–(d)) exhibit a line with a slope close to 90° along the imaginary axis (Z''), characteristic of an ideally polarizable electrode. A slight deviation from the straight line along the imaginary axis (Z'') is apparent when potential is 0.13 V (versus Hg/HgO), suggestive of a non-ideally polarizable electrode. While at potential of 0.6 V, only two circles displayed and line characteristic disappeared, which is characteristic of desorption of adatoms H_{ads} [34]. This change of impedance spectroscopy with the potential illustrate that the pseudo-capacitance involved in the process arises from under-potential deposition (UPD) of H_3O^+. And the proper potential range, in which electrode can generate desirable capacitance, is among 0.1 and 0.6 V. These results are good agreement with that

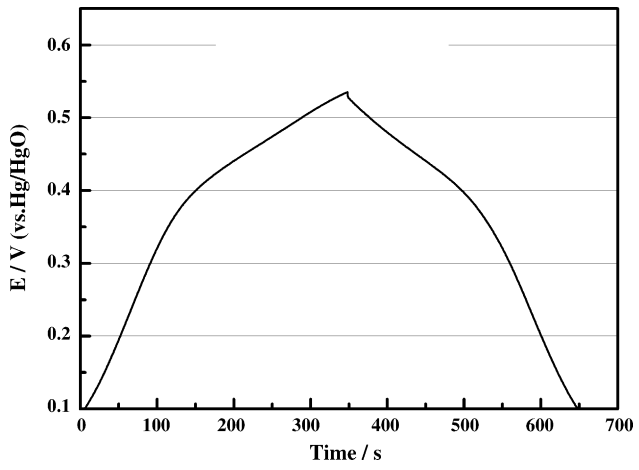

Fig. 4. Galvanostatical charge/discharge curve of nano-cobalt silicate hydroxide electrode in 6 M KOH solution at 5.7 mA cm^2 constant current.

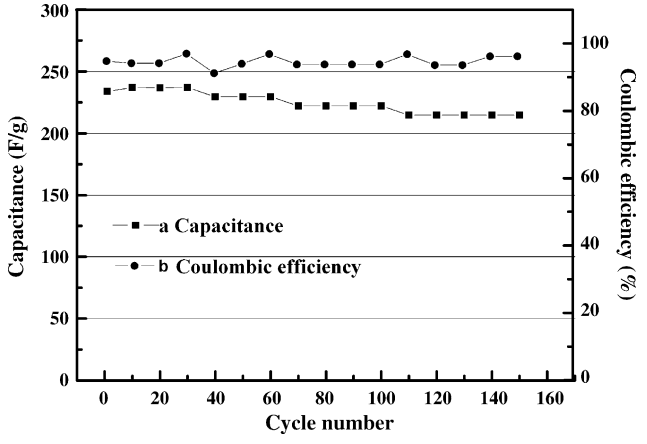

Fig. 5. Variation of capacitance and coulombic efficiency with cycle number for the nano-cobalt silicate hydroxide electrode in 6 M KOH solution with 5.7 mA cm^2 charge/discharge current: (a) capacitance; (b) coulombic efficiency.

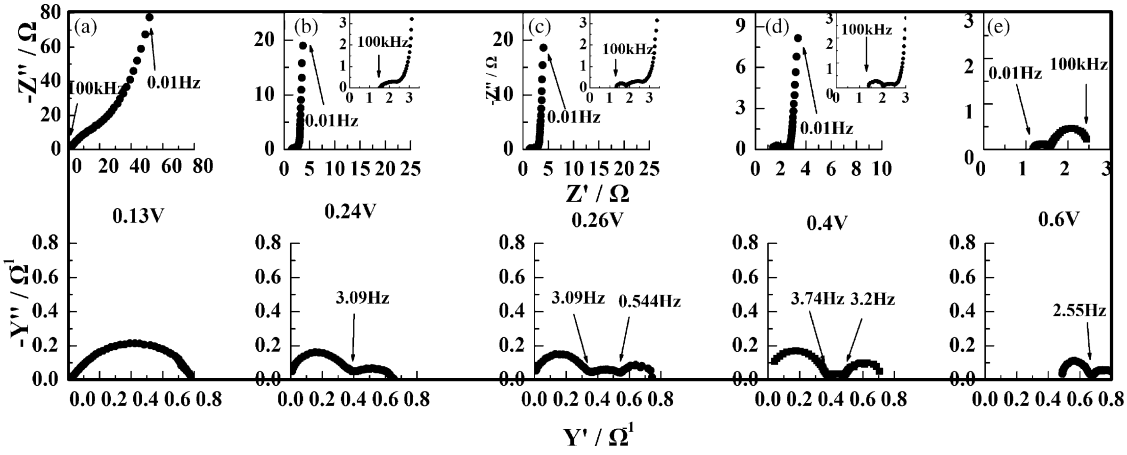

Fig. 6. Nyquist plots for the nano-cobalt silicate hydroxide electrode in 6 M KOH solution at different potentials: (a) 0.13 V; (b) 0.24 V; (c) 0.26 V; (d) 0.4 V; (e) 0.6 V.

of CV measurements. At high frequencies, impedance behave like a resistance R for all potentials tested. At low frequency, the imaginary part of the impedance sharply increases and the plot tends to a vertical line, characteristic of capacitive behavior only except that of at 0.6 V. In the middle frequency range the plot is quite linear. The crossing of this line with the low-frequency vertical line defines the "knee frequency" below this frequency; the whole capacitance is reached, for higher values, the capacitance strongly dependents on the frequency [35].

The frequency dependence of the magnitude $|Z|$, the phase angle Φ, (Bode plots) at different applied potentials is shown in Fig. 7. The Bode plots can also be separated into the high frequency, medium frequency, and low-frequency regions. At the high-frequency regions, $|Z|$ is weakly dependent on frequency, and the phase angle is near zero. The knee frequency in the admittance complex-plane plots (shown in Fig. 6) is between 0.544 and 3.2 Hz, which characterize the lower limit of high frequency region. The region where the $\log f - \log |Z|$ plot displays a slope close to -1 (corresponding to line part in Nyquist plot), and $90^\circ < \Phi < 45^\circ$ in the $\log f - \log \Phi$ plot, can be regarded as the low-frequency region. The characteristic of near -1 slope (Fig. 7(b)–(d)) indicates that this region is typical of capacitive behavior. The frequency where $\Phi = -45^\circ$ ($f_\Phi = -45^\circ$) can be recognized as the frequency response to the ideally capacitive behavior (capacitor response frequency). The $f_\Phi = 45^\circ$ values ranged from 0.03 to 0.08 Hz, giving the response time of the capacitor as 30–10 s. Except the case of Fig. 7(e), the maximum specific capacitance was calculated from the low-frequency data using the equation $Z'' = (2\pi fC)^{-1}$ where Z'' is the imaginary part of the impedance, f the frequency, and C is the capacitance. The specific capacitance at different potentials calculated from the Z'' value at the lowest frequency (f) 0.01 Hz is 30, 120, 120, and 270 F g^{-1}, respectively, for the electrode at different applied potentials.

Based on the above discussion, combining the shape of the impedance spectroscopy and characteristic of capacitor, Equivalent circuits in Fig. 8 can be employed to further analyze the electrode process occurred during the operation.

Supercapacitor oscillates between two states: resistance at high frequencies and capacitance at low frequencies. Between these two states it behaves like a resistance–capacitance (RC) transmission line circuit [36–38]. The equivalent circuit for the test system involves the following circuit elements: the double-layer capacitance C_{dl}, a Faradaic resistance R_F, corresponding to the reciprocal of the potential-dependent charge-transfer rate in the above processes, and a pseudo-capacitance,

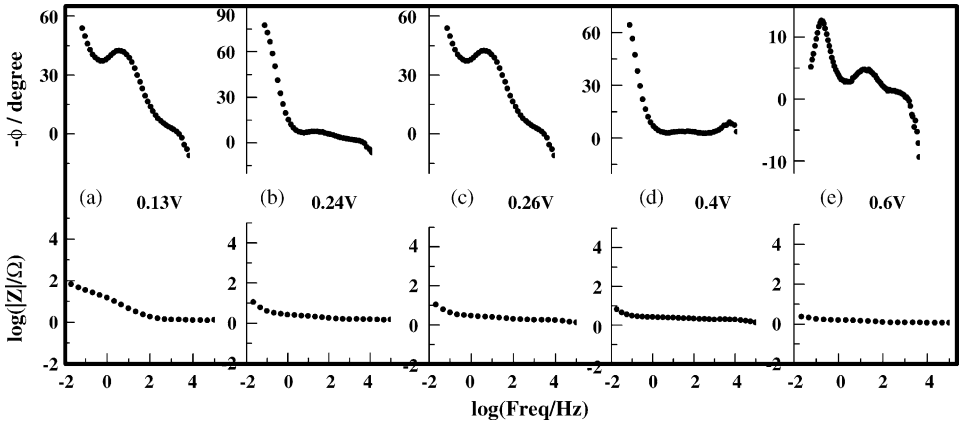

Fig. 7. Bode plots for the nano-cobalt Silicate hydroxide electrode in 6 M KOH solution at different potentials: (a) 0.13 V; (b) 0.24 V; (c) 0.26 V; (d) 0.4 V; (e) 0.6 V.

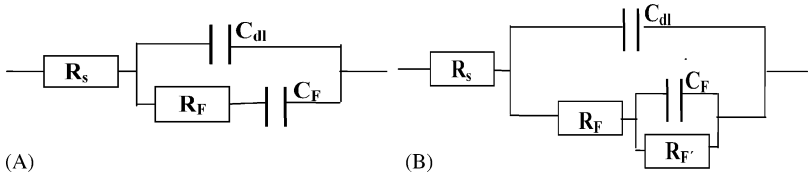

Fig. 8. Equivalent circuits for modeling the impedance of nano-cobalt silicate hydroxide electrode.

C_F. $C_F = q_1(d\theta/dV)$ in the general case where q_1 is the charge required for formation or desorption of the species in a redox process [39]. Solution resistance, R_s, is usually combined in series with the Faradaic impedance involving R_F and C_F (Fig. 8(A)). This case corresponds to the experimental results at 0.13, 0.24, 0.26, and 0.4 V (Fig. 6(a)–(d)).

The interfacial part, Z, of the overall impedance can been given by

$$\frac{1}{Z} = \frac{1}{1/j\omega C_{dl}} + \frac{1}{R_F + (1/j\omega C_F)} \tag{1.1}$$

$$\frac{1}{Z} = j\omega C_{dl} + \frac{j\omega C_F}{j\omega R_F C_F + 1} \tag{1.2}$$

For Eq. (1.2), two limiting cases arise: (i) At very low frequencies ($\omega \to 0$), and/or low R_F,

$$\frac{1}{Z} = j\omega(C_{dl} + C_F) \tag{1.3}$$

i.e. C_{dl} and C_F are effectively added as in a simple parallel arrangement and the measured $C = C_{dl} + C_F$, which is a good agreement with the result analysis of constant charge/discharge. (ii) At sufficiently high frequencies ($j\omega R_F C_F \gg 1$)

$$Z = \frac{R_F}{(1 + j\omega R_F C_{dl})} \tag{1.4}$$

$$Z = \frac{R_F}{1 - \omega^2 R_F^2 C_{dl}^2} - \frac{j\omega R_F^2 C_{dl}}{1 - \omega^2 R_F^2 C_{dl}^2} \tag{1.5}$$

The further limiting case for (ii) when $j\omega C_{dl} \gg 1/R_F$ is

$$Z = \frac{1}{j\omega C_{dl}} \tag{1.6}$$

i.e. the impedance is determined by C_{dl} at sufficiently high frequencies, combined with R_s.

In the case when the potential is beyond the UPD range, another Faradic potential-dependent $R_{F'}$ arises in parallel with C_F, corresponding to the equivalent circuit (Fig. 8(B)). This situation corresponds to Fig. 6(e), suggestive of overcharge of the pseudo-capacitance where a continuous Faradaic reaction takes place in the overpotential region for the process. The Faradaic, R_F, in the above circuit corresponds to the reciprocal of the potential-dependent rate, which enables the intermediates that give rise to C_F to become desorbed (i.e. H_{ads} desorption). There can then be two semicircles and three intercepts on the Z'-axis (Nyquist plot), which can be seen in the case of the electrode at 0.6 V. This analysis also suggested that the redox process involved in the test system is underpotential deposition (UPD) of H_3O^+, which further confirms the correctness of above speculation in the CV experiments.

4. Conclusion

Nano-cobalt silicate hydroxide ($Co_3[Si_2O_5]_2[OH]_2$) has been prepared and employed to supercapacitor in this study. XRD and TEM studies confirmed the pure hexagonal phase of the sample with uniform nanometer particle size distribution. Cyclic voltammeter (CV) and galvanostatic charge/discharge studies were also performed, and the results reveal that the cobalt silicate hydroxide-based electrode has stable electrochemical capacitor properties between potential range of 0.1–0.55 V with a maximum specific capacitance of 237 F g^{-1} in alkaline solution. After150 charge/discharge cycles, the synthesized material shows high efficiency and stability. Detailed electrochemical impedance spectra (EIS) investigation illustrates that the pseudo-capacitance of the test electrode was caused by underpotential deposition of H_3O^+ at the electrode surface. As-prepared cobalt silicate hydroxide with good electrochemical capacitor properties displayed in this study may be a promising electrode material for supercapacitor.

Acknowledgement

This work is supported by the National Natural Science Foundation of China (no. 60471014).

References

[1] A. Burke, J. Power Sources 37 (2000) 91.
[2] A. Nishino, J. Power Sources 60 (1996) 137.
[3] M. Carlen, R. Kotz, Electrochim. Acta 45 (2000) 2483.
[4] R.A. Huggins, Solid State Ionics 179 (2000) 134.
[5] A.B. Fuertes, F. Pico, J.M. Rojo, J. Power Sources 133 (2004) 329.
[6] U. Fischer, R. Saliger, V. Rock, J. Porous Mater. 4 (1997) 281.
[7] E. Frack owiak, F. Beguin, Carbon 40 (2002) 1775.
[8] H.S. Kim, N. Branko, B.N. Popov, J. Power Sources 52 (2002) 104.
[9] J.H. Jiang, A. Kucernak, Electrochim. Acta 47 (2002) 2381.
[10] K.W. Nam, K.B. Kim, J. Electrochem. Soc. 149 (2002) A346.
[11] M. Mastragostino, C. Arbizzani, F. Soavi, J. Power Sources 97/98 (2001) 812.
[12] A. Bard, L.R. Faulkner, Electrochemical Methods, John Wiley and Sons, New York, 2000.
[13] J. Gamby, P.L. Taberna, P. Simon, J. Power Sources 101 (2001) 109.
[14] H.S. Kim, N. Branko, B.N. Popov, J. Power Sources 104 (2002) 52.
[15] J.W. Long, K.E. Swinder, C.I. Merzbacher, D.R. Rolison, Langmuir 15 (1999) 780.
[16] D. Miousse, A. Lasia, J. New Mater. Electrochem. Syst. 71 (1999) 2.
[17] J.P. Zheng, P.J. Cygan, T.R. Jow, J. Electrochem. Soc. 142 (1995) 2669.
[18] C. Niu, E.K. Sichel, R. Hoch, D. Moy, H. Tennent, Appl. Phys. Lett. 70 (1997) 1480.

[19] A. Corma, Chem. Rev. 97 (1997) 2373.
[20] R.M. Hazen, R.T. Downs, L.W. Finger, Science 272 (1996) 1769.
[21] J.S. Beck, J.C. Vartuli, W.J. Roth, M.E. Leonowicz, C.T. Kresge, K.D. Schmitt, C.T.-W. Chu, D.H. Olson, E.W. Sheppard, S.B. McCullen, J.B. Higgins, J.L. Schlenkert, J. Am. Chem. Soc. 114 (1992) 10834.
[22] D.Y. Zhao, J.L. Feng, Q.S. Huo, N. Melosh, G.H. Fredrickson, B.F. Chmelka, G.D. Stucky, Science 279 (1998) 548.
[23] Z.T. Zhang, Y. Han, L. Zhu, R.W. Wang, Y. Yu, S.L. Qiu, D.Y. Zhao, F.S. Xiao, Angew. Chem. 113 (2001) 1298.
[24] F.S. Xiao, Y. Han, Y. Yu, X.J. Meng, M. Yang, S. Wu, J. Am. Chem. Soc. 124 (2002) 888.
[25] P.D. Yang, T. Deng, D.Y. Zhao, P.Y. Feng, D. Pine, B.F. Chmelka, G.M. Whitesides, G.D. Stucky, Science 282 (1998) 2244.
[26] P.D. Yang, D.Y. Zhao, D.I. Margolese, B.F. Chmelka, G.D. Stucky, Nature 396 (1998) 152.
[27] T. Sun, J.Y. Ying, Nature 389 (1997) 704.
[28] B.V. Tilak, V.I. Birss, J. Wang, C.-P. Chen, S.K. Rangarajan, J. Electrochem. Soc. 148 (2001) 112.
[29] F. Lufrano, P. Staiti, M. Minutoli, J. Power Sources 124 (2003) 314.
[30] W. Sugimoto, H. Iwata, Y. Yasunaga, Y. Murakami, Y. Takasu, Preparation of ruthenic acid nanosheets and utilization of its interlayer surface for electrochemical energy storage, Angew. Chem. Int. Ed. 42 (2003) 4092.
[31] P.L. Taberna, P. Simon, J.F. Fauvarque, J. Electrochem. Soc. 150 (2003) 292.
[32] Y.R. Nian, H.S. Teng, J. Electroanal. Chem. 540 (2003) 119.
[33] T.L. Momma, X. Osaka, T. Ushio, Y. Sawada, J. Power Sources 60 (1996) 249.
[34] B.E. Conway, Electrochemical Supercapacitors: Scientific, Fundamentals and Technological Application, Plenum, New York, 1999, p. 555.
[35] M. Keddamand, H. Takenouti, Electrochemical capacitors II, in: F.M. Delvick, D. Ingersoll, X. Andriev, K. Naoi (Eds.), Proceedings of the Electrochemical Society Series, PV 96–25, Pennington, NJ, 1996, p. 220.
[36] D. Quand, H. Shi, J. Power Sources 74 (1998) 99.
[37] H.K. Song, Y.H. Jung, K.H. Lee, L.H. Dao, Electrochim. Acta 44 (1999) 3513.
[38] H. Keiser, K.D. Beccu, M.A. Gutjahr, Electrochim. Acta 12 (1976) 539.
[39] B.E. Conway, Electrochemical Supercapacitors: Scientific, Fundamentals and Technological Application, Plenum, New York, 1999, p. 520.